Consolidating boundary methods for finding the eigenstates of billiards

Doron Cohen[1]**, Natasha Lepore**[2] **and Eric J Heller**[2,3]

[1] Department of Physics, Ben-Gurion University, Beer-Sheva, Israel
[2] Department of Physics, Harvard University, Cambridge, MA, USA
[3] Department of Chemistry and Chemical Biology, Harvard University, Cambridge, MA, USA

Abstract
The plane-wave decomposition method, a widely used means of numerically finding eigenstates of the Helmholtz equation in billiard systems is described as a variant of the mathematically well-established boundary integral method (BIM). A new unified framework encompassing the two methods is discussed. Furthermore, a third numerical method, which we call the gauge freedom method is derived from the BIM equations. This opens the way to further improvements in eigenstate search techniques.

PACS number: 05.45.Mt

1. Introduction

Solving the Helmholtz equation within a domain given Dirichlet boundary conditions is of great interest to both physicists [1] and engineers. Firstly, the Helmholtz equation is the simplest example of a *wave equation*. Furthermore, this equation may be used to describe acoustic waves, microwave systems, and in particular the wavefunction of a quantal particle inside nanoscale devices [2] such as quantum dots, where the motion of the electrons can be regarded as a free motion within a box. For this reason it has become a prototype problem in studies of quantum chaos.

Of particular interest are the wavefunctions $\Psi(x)$ of a stationary particle in a two-dimensional box (a so-called billiard system). These wavefunctions are solutions of the homogeneous Helmholtz equation $\mathcal{H}\Psi(x) = 0$, where the differential operator $\mathcal{H}$ is defined as

$$\mathcal{H} = -\nabla^2 - k^2. \tag{1}$$

Note that for the special case $k = 0$, the Helmholtz equation reduces to Laplace's equation. Given a closed boundary we can ask whether this equation has a non-trivial solution that satisfies Dirichlet boundary conditions $\Psi(x) = 0$.

Two main numerical strategies have been suggested to date in the literature in order to find the eigenstates of the Helmholtz equation (for more comprehensive reviews and references, see for example [3–5]). The first strategy can be described as a 'Laplacian diagonalization'. A basis is selected such that the functions it contains satisfy the Dirichlet boundary conditions. For example, in some cases one can use conformal mapping to determine a basis [6] (and see also [7]). The Laplacian operator is then written in this basis and diagonalized. Numerically, some truncation is required, and the diagonalization only determines all the eigenstates up to some maximum wavenumber k_{max}. Thus, the Laplacian diagonalization strategy is inherently limited, and cannot be used for the purpose of finding high-lying eigenstates.

The second numerical strategy, which is the object of this paper, can be described as a 'boundary approach'. This strategy is based on the observation that the eigenfunctions are completely determined by their behaviour at the boundary. The boundary methods use basis functions that satisfy the Helmholtz equation inside the billiard at fixed k. A linear combination of the basis functions is then selected such that the boundary conditions are satisfied. Thus, in order to find the eigenstates, one only needs to study the small k window that contains the energy range of interest. Therefore the method is naturally suitable for the purpose of finding high-lying eigenstates. For 2D billiards, the Laplacian diagonalization requires 2D grid calculations. This is a heavy numerical task. The boundary approach, on the other hand reduces the calculations to a 1D boundary grid.

In the quantum chaos community, two boundary methods are commonly employed. The first one is referred to as the boundary integral method (BIM) [8], while the other is what we call here the decomposition method (DEM), of which the plane-wave decomposition method (PWDM) [9] is a special case. Extensions of the standard PWDM have been used in [10, 11] and in [5].

Usually, the BIM and the PWDM are considered to be two independent self-contained procedures. Several studies have been done in order to compare their capabilities [12]. While the BIM equation is exact, its convergence is very slow (power law in the number b of discretization points per half-wavelength). On the other hand while the PWDM is mathematically limited (e.g. the maximal b is semiclassically determined), it is still found to be extremely efficient in practice. Hence there is definitely a need to develop hybrid boundary methods.

In this paper, we adopt a new point of view through which we regard the BIM and the DEM as sequences of four independent steps. By doing so, we make the observation that the DEM and the BIM are strongly related: *the two procedures are based on the diagonalization of literally the same matrix!* As a bridge between them, we will highlight an intermediate strategy which we call the gauge freedom method (GFM). In a follow-up paper, this framework will lead the way to improved eigenstate search techniques combining the strengths of the two boundary methods [13].

Our unified description of the different boundary methods can be summarized by the following set of four steps that are common to the BIM and the DEM, and as we will show later, to the GFM:

- choice of a set of basis functions $F_j(x; k)$;
- definition of the Fredholm matrix $\mathbf{A}_{js}(k)$;
- procedure for construction of the wavefunction Ψ_r;
- definition of the quantization measure $S(k)$.

The first step consists of selecting a set of basis functions $F_j(x; k)$ labelled $j = 1, \ldots, N$. All boundary methods rely on basis functions that satisfy the Helmholtz equation *inside* the billiard. Thus, a superposition of such basis functions is an eigenfunction if it vanishes along

the boundary. The choices of bases that correspond to the PWDM, to the primitive version of the BIM and to the simplest variation of the GFM are as follows:

$$F_j(x; k) = \cos(\phi_j + kn_j \cdot x) \qquad \text{PWDM} \qquad\qquad (2)$$

$$F_j(x; k) = Y_0(k|x - x_j|) \qquad \text{Y0-BIM} \qquad\qquad (3)$$

$$F_j(x; k) = J_0(k|x - x_j|) \qquad \text{J0-GFM}. \qquad\qquad (4)$$

For the purpose of numerical treatment we represent the boundary by a set of points x_s with $s = 1, \ldots, M$. In practice, we choose a set of M equally spaced points, so that the spacing is $\Delta s = L/M$ where L is the perimeter of the billiard. Depending on the details of the numerical strategy, the number of points along the boundary is either taken to be equal to the number of basis functions ($M = N$), or it may be larger ($M > N$). The Fredholm matrix is defined as

$$\mathbf{A}_{js}(k) \equiv F_j(x_s; k). \qquad\qquad (5)$$

Given k, one may perform the singular value decomposition (SVD) of the matrix $\mathbf{A}$. The smallest singular value is the one which we care about. If it is a minimum at a given k, then the billiard system is likely to have an eigenvalue at that energy.

In the third step, the left and the right eigenvectors of the smallest singular value (Φ_s and C_j, resp.) are used to construct a wavefunction Ψ_r through a linear transformation. We select a grid of points X_r on which the wavefunction $\Psi_r \equiv \Psi(X_r)$ is calculated. In the DEM, the left eigenvector C is used for the purpose of this construction, and the linear transformation which is applied is

$$\Psi_r = \sum_j \mathsf{C}_j \mathbf{F}_{jr} \qquad\qquad (6)$$

where $\mathbf{F}_{jr} \equiv F_j(X_r; k)$. Note that C contains the expansion coefficients of $\Psi(x)$ in the chosen basis $F_j(x; k)$. For the BIM, the right eigenvector Φ is used in order to build the wavefunction, and the linear transformation in this case is

$$\Psi_r = \sum_s \mathbf{G}_{rs} \Phi_s \qquad\qquad (7)$$

where $\mathbf{G}_{rs}$ is the discretized version of the Green function. Thus, the vector Φ_s represents a 'charge' that is distributed along the boundary.

In the final step, a measure $S(k)$ is defined such that $S(k) = 0$ if k is an eigenvalue and $S(k) > 0$ otherwise. In practice, the eigenvalues are determined by searching for the local minima of $S(k)$. By construction, the wavefunction which was built in the third step satisfies the Helmholtz equation inside the boundary. Therefore, the most natural choice of $S(k)$ is the tension, the sum of the square of the wavefunction along the boundary. The tension is thus a measure for the roughness of the constructed $\Psi(x)$ along the boundary. This definition of $S(k)$ is traditionally used with the PWDM. Other possibilities for the measure include the smallest singular value, and the Fredholm determinant of $\mathbf{A}$. These two latter choices of $S(k)$ are the ones that are usually associated with the BIM. In section 4 we discuss the mathematical equivalence of the three possible measures, and compare their respective numerical effectiveness.

1.1. Outline

In section 2, we give a concise presentation of the BIM and the related GFM. Our derivation of the BIM equation contains some significant improvements over previous ones. Most
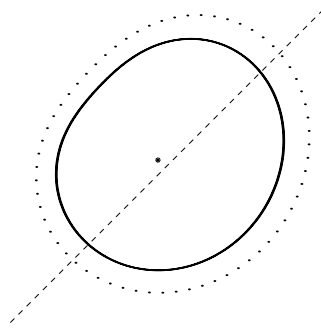
Figure 1. Full line: the 'pond' shape. The polar equation of the Pond shape is $r = 1 + 0.2 * \cos(\theta + 0.9 * \cos(\theta))$. Hence its perimeter is $L = 6.364$. Dashed line: the cross-section line that is used, e.g. in figure 3(*c*). Dots: the 'outer boundary' which is used for the BIM tension calculation (see section 3.1). The transverse distance between the actual boundary and the outer boundary was chosen in most cases to be $\Delta L \sim 10\Delta s$. Star: the selected point which is used in Heller's implementation of the PWDM method.

importantly, it naturally leads to the existence of the GFM. Furthermore, we have succeeded in avoiding the use of the complicated 'regularized' method of images, which was the major ingredient in the derivation of [12].

Strategies for constructing the wavefunction are discussed in section 3. An explanation of the Green function method is given, as well as a critical discussion of the DEM and its numerical variants.

Section 4 explores the practicality of using different choices for the quantization measure. In particular, it is demonstrated that a tension measure can be defined not only for the PWDM, but for the case of the BIM as well. An important issue emerges as to whether the quantization measures can be used to determine the error in the bulk wavefunction. We address this issue, and also make a comparison between the numerical accuracies of the BIM and of the PWDM.

Section 5 explains how the GFM bridges the gap between the BIM and the DEM. It is found that for any DEM, an associated GFM exists, whereas the converse statement is not true.

The shape that we have studied numerically is presented in figure 1. We have used the cornerless, generic 'pond' shape in order to avoid the range of problems that arise with more complicated geometries. These problems are the subject of a follow-up study [13], where we suggest mixed BIM/DEM methods for finding eigenfunctions. This is done using the above theoretical framework, while regarding the 'pond' shape as a reference against which to judge the effectiveness of our efforts. Another direction of research is related to billiards in magnetic fields [14].

For the convenience of the reader, our numerical notation is concentrated in table 1. Further information about figure 1, table 1 and the numerical analysis is integrated within the main text.

2. The BIM and the GFM

The gist of the BIM is that, from the knowledge of the gradient of the wavefunction on the boundary and from Green's theorem, it is possible to find the value of the wavefunction everywhere inside the billiard. We give a derivation of this method in this section. This procedure will lead us naturally to the existence of the GFM.

Table 1. Notation.

x_s = Vector of boundary points
x_s = Vector of outer-boundary points
X_r = Vector of interior grid points
X_0 = Randomly selected interior point
Ψ_r = Wavefunction on the grid points
Ψ_s = Wavefunction on the boundary points
Φ_s = 'Charge' along the boundary
$\|\Psi_r\|$ = Norm of the wavefunction (see section 3)
$\|\Psi_s\|$ = Tension of the wavefunction (see section 3)
$n(s)$ = Unit normal at the boundary point x_s
$\mathbf{w}_s = (1/(2k^2))n(s) \cdot x_s$
$\mathbf{G}_{rs} = G(X_r, x_s)$
$\mathbf{A}_{j0} = F_j(X_0; k)$
$\mathbf{A}_{js} = F_j(x_s; k)$
$\mathbf{D}_{js} = \partial F_j(x_s; k)$
$\mathbf{B}_{ij} = \Delta s \sum_s \mathbf{w}_s \mathbf{D}_{is}\mathbf{D}_{js} = \Delta s(\mathbf{D}\mathbf{w}\mathbf{D}^\dagger)_{ij}$
$\mathbf{T}_{ij} = \Delta s \sum_s \mathbf{A}_{is}\mathbf{A}_{js} = \Delta s(\mathbf{A}\mathbf{A}^\dagger)_{ij}$

The free space Green function $G(x, x')$ is defined by the equation $\mathcal{H}G(x, x') = \delta(x - x')$. The most general solution can be written as

$$G(x, x') = -\tfrac{1}{4}Y_0(k|x - x'|) + \mathcal{C}(x, x') \tag{8}$$

where $\mathcal{C}(x, x')$ is any solution of the homogeneous equation $\mathcal{H}\mathcal{C}(x, x') = 0$. Note that in the electrostatic limit $k \to 0$ we have $G(x, x') = -(1/(2\pi)) \ln(r) + \mathcal{C}$, where $\mathcal{C}$ is a constant[4]. We shall refer to the choice of $\mathcal{C}(x, x')$ as gauge freedom. This term is at the core of the GFM.

By the definition of the Green function, it follows that a solution of the generalized Poisson–Laplace (GPL) equation $\mathcal{H}\Psi(x) = \rho(x)$ is[5]

$$\Psi(x) = \int G(x, x')\rho(x')\,\mathrm{d}x'. \tag{9}$$

We refer to $\rho(x)$ as the 'charge density', in analogy with its electrostatic equivalent.

We shall use the notation $\Phi(s)$ in order to refer to the (surface) charge density upon the boundary. In the latter case, the above equation reduces to

$$\Psi(x) = \oint G(x, x(s))\Phi(s)\,\mathrm{d}s \tag{10}$$

where s parametrizes the boundary.

2.1. The BIM

Let us assume that k is an eigenvalue of the billiard. In such a case, there exists a non-vanishing $\Psi(x)$ inside the boundary that satisfies $\Psi(x) = 0$ on the boundary. It can be shown from Green's theorem that the interior wavefunction satisfies equation (10) with

$$\Phi(s) = \partial_-\Psi(x(s)) \equiv \lim_{x\uparrow x(s)} n(s) \cdot \nabla\Psi(x) \tag{11}$$

where $n(s)$ is the outward pointing normal at point s, and ∂_- is used for the normal derivative evaluated inside the billiard walls.

---

[4] We assume here the usual free space boundary conditions used in electrostatics.

[5] Note that equation (9) always gives 'a solution' of the GPL equation. This is true irrespective of the choice of boundary conditions and Green function.
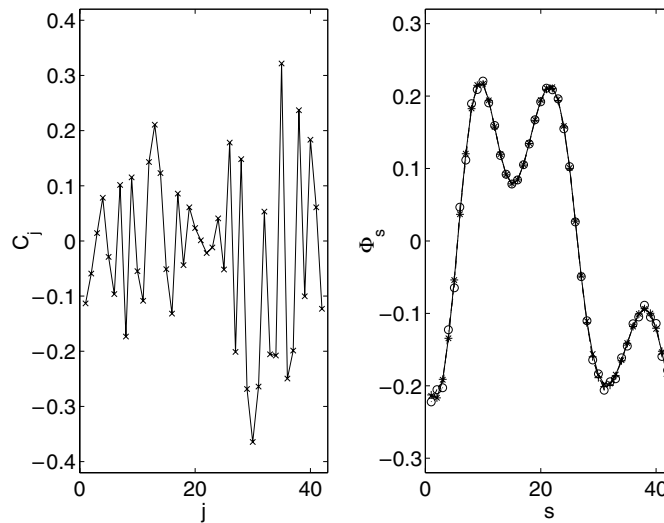
Figure 2. The eigenvectors of the Fredholm matrix (equation (5)) are found for $k = k_n = 6.827\,545\,928\,676\,94$. Right plot: the right eigenvector Φ. The symbols ($\times$) and (+) and ($\circ$) correspond respectively to the PWDM choice of equation (2), to the H1-BIM choice of equation (B.3) and to the J0-GFM choice of equation (4). Left plot: the left eigenvector C for the PWDM Fredholm matrix.

In electrostatics, it is known that forcing the scalar potential to be zero on the boundary induces a boundary charge. From Green's theorem, the induced charge is proportional to the normal component of the electric field. Here the wavefunction acts as the equivalent of the scalar potential. Similar to the electrostatic case, there exists an induced 'boundary charge', which in this case is proportional to the normal derivative of the wavefunction.

The BIM is based on the fact that if an eigenstate exists, then there also exists a charge density $\Phi(s)$ given by equation (11), such that equation (10) is satisfied. On the boundary, equation (10) yields

$$\int G(x(j), x(s)) \Phi(s)\, ds = 0 \qquad \text{(BIM equation)}. \qquad (12)$$

Thus, having an eigenstate $\Psi(x)$ implies that the kernel $G(x(j), x(s))$ has an eigenvector $\Phi(s)$ that corresponds to a zero eigenvalue. Figure 2 shows an example of a boundary charge density $\Phi(s)$ that was found via the BIM equation (for more details, see the next section). The converse is also true: once a non-trivial charge density is found that satisfies equation (12), the associated eigenstate can be constructed using equation (10). We discuss this construction issue in more detail in the next section.

For numerical purposes, it is convenient to use the discretized version equation (7) of the above formula. The BIM equation can then be written as the matrix equation $\mathbf{A}\Phi = 0$, where $\mathbf{A}_{js} = G(x(j), x(s))$. The gauge term $\mathcal{C}(x, x')$ allows some freedom in the determination of the Green function. Using the Neumann–Bessel function $Y_0(k|x - x'|)$ for the Green function, one obtains the matrix $\mathbf{A}_{js}$ as defined by equation (5) with (3). Another possibility is to use the Hankel–Bessel function $H_0(k|x - x'|)$. Accordingly, we will distinguish between the Y0-BIM version and the H0-BIM version. We shall later discuss the numerical implication of using the complex $H(k|x - x'|)$ rather than the real $Y(k|x - x'|)$.

The primitive BIM uses equation (12) literally. However, this version of the BIM is not the one that is generally favoured because $G(x(j), x(s))$ is singular for $x(j) \to x(s)$, leading to

some difficulty in determining the diagonal matrix elements of $\mathbf{A}_{js}$. Therefore, other versions of the BIM have become popular (see appendices B and C).

2.2. The GFM

The GFM is a different strategy to obtain the charge density $\Phi(s)$. Rather than using the BIM equation (12) or one of its variants, a gauge freedom argument is invoked in order to introduce a new type of equation (equation (13)). It is clear that equation (12) should be valid for *any* choice of gauge. In other words, equation (12) should be satisfied for any Green function (equation (8)), regardless of the choice of $\mathcal{C}(x, x')$. Thus, for a given $\mathcal{C}(x, x')$, the charge density $\Phi(s)$ must satisfy the equation

$$\int \mathcal{C}(x(j), x(s))\Phi(s)\,\mathrm{d}s = 0 \qquad \text{(GFM equation).} \qquad (13)$$

For example, we may take $\mathcal{C}(x, x') = J_0(k|x - x'|)$, and we shall refer to this version of GFM as J0-GFM. For numerical purposes, it is once again convenient to discretize the integral expression, which can then be written as the matrix equation $\mathbf{A}\Phi = 0$.

The kernel $\mathbf{A}_{js} = J_0(k|x - x'|)$ of the J0-GFM is non-singular, and very well behaved. Thus, the J0-GFM method, unlike the Y0-BIM, provides an extremely convenient way of obtaining the eigenvalues of the Helmholtz equation. Figure 2 shows an example of a charge density that was found via the J0-GFM equation (for more details, see the next section). The result is indistinguishable from the charge density generated by the traditional H1-BIM. (We note however that the J0-GFM method has certain numerical limitations that we are going to discuss later.) Once the eigenvector $\Phi(s)$ is found via the GFM equation, we can proceed as with the traditional BIM, and construct the wavefunction $\Psi(x)$ using equation (7).

3. Constructing the wavefunction

In this section we explain how a wavefunction $\Psi(x)$ is constructed for a given k. It is assumed that k is an eigenvalue. The (numerical) question of how to determine the eigenvalues $k = k_n$ is deferred to section 4.

3.1. Green function method (equation (7))

Both the BIM and GFM make use of equation (7) in order to construct the wavefunction. In order to find the charge vector Φ_s the BIM equation (equation (12)) and the GFM equation (equation (13)) are written as the matrix equation $\mathbf{A}\Phi = 0$. The only difference between the two is in the expression for $\mathbf{A}$. Given k, one performs the SVD of the matrix $\mathbf{A}$. Figure 4 shows an example of the output of such a SVD procedure. One then finds the right eigenvector Φ that corresponds to the *smallest* singular value.

Once the charge vector Φ_s has been determined, as in the example of figure 2, one can construct the wavefunction using equation (7). For the Green function (8), it is most natural to use the simplest gauge ($\mathcal{C} = 0$). If k is known to be an eigenvalue, then any gauge should give the same result, and in particular, the wavefunction associated with any complex part of the Green function (such as that of the Hankel function) should vanish. The outcome of the Green function method is illustrated in figure 3.

It is natural to ask how the constructed wavefunction $\Psi(x)$ looks like outside the boundary. The answer turns out to be $\Psi(x) = 0$. For completeness, we give a proof of this statement. Let us define an extended function $\Psi_{\text{ex}}(x)$ such that $\Psi_{\text{ex}}(x) = \Psi(x)$ inside and $\Psi_{\text{ex}}(x) = 0$ outside the boundary. We would like to show that $\Psi(x)$ as defined by
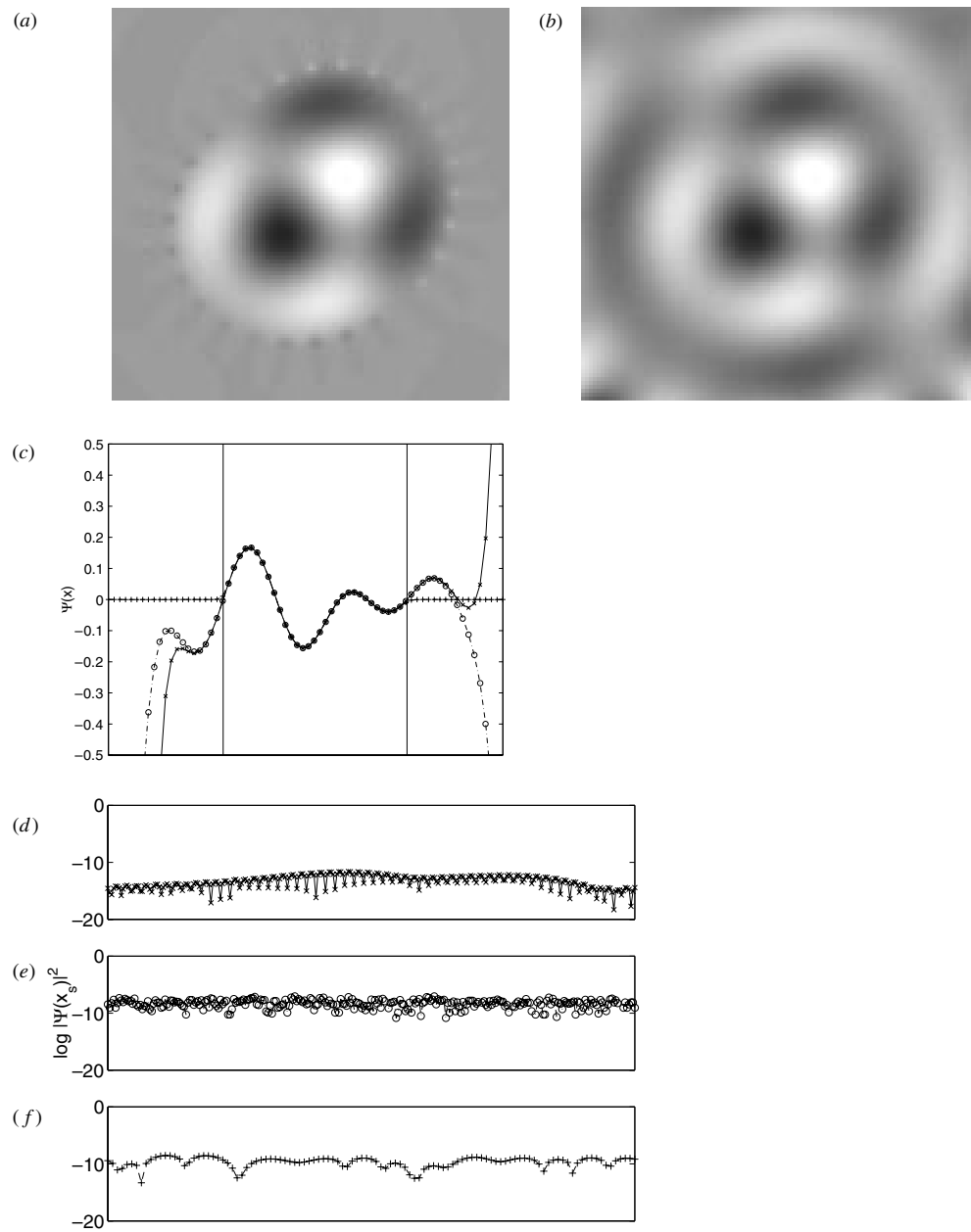
(a)

(b)

(c)

(d)

(e)

(f)

Figure 3. The eigenfunction at $k = k_n$ is found using the eigenvectors of figure 2. (*a*) An image of $\Psi(x)$ using equation (7). (*b*) The same using PWDM and equation (6). (*c*) Plot of $\Psi(x)$ along the cross-section line of figure 1. The vertical lines indicate the location of the boundary. The wavefunctions that correspond to images (*a*) and (*b*) are shown with (+) and (×), respectively. We also show with (○) the wavefunction that is obtained using J0-GFM and equation (6). (*d*)–(*f*) Plots of $\log(|\Psi(x)|^2)$ along the boundary. The symbols are as in (*c*).

equation (10) is also equal to $\Psi_{ex}(x)$ outside the boundary. It is clear that $\Psi(x)$ is a solution of the GPL equation by construction (see the discussion following equation (9)). In the next paragraph, we argue that $\Psi_{ex}(x)$ is a solution of the *same* GPL equation. It follows that the

difference $R(x) = \Psi(x) - \Psi_{\mathrm{ex}}(x)$ is a solution of the Helmholtz equation in free space. From the definition of $\Psi_{\mathrm{ex}}(x)$, we have $R(x) = 0$ in the interior region, which implies by the unique continuation property that $R(x) = 0$ over all space.

The proof that $\Psi_{\mathrm{ex}}(x)$ is a solution of the GPL equation with a charge density given by equation (11) goes as follows. By construction, $\Psi_{\mathrm{ex}}(x)$ satisfies the GPL equation inside as well as outside the boundary. All we have to show is that it also satisfies the GPL equation across the boundary. The latter statement is most easily established by invoking Gauss's law. This approach is valid because at short distances, $G(x, x')$ coincides with the electrostatic Green function. Thus, the gradient of $\Psi_{\mathrm{ex}}(x)$ corresponds, up to a sign, to the electric field. Gauss's law implies that the electric field should have a discontinuity equal to the charge density $\Phi(s)$. Indeed, $\Psi_{\mathrm{ex}}(x)$ is consistent with this requirement.

3.2. Decomposition method (equation (6))

The other procedure for constructing the wavefunction is to use the DEM equation (6). The idea is to regard $F_j(x; k)$ as a basis for the expansion

$$\Psi(x) \approx \sum_j \mathsf{C}_j F_j(x; k). \tag{14}$$

Any such superposition at fixed k is a solution of the Helmholtz equation within the interior region. Thus, in order to satisfy the Dirichlet boundary conditions, one looks for a vector C of expansion coefficients that satisfy $\mathsf{C}\mathsf{A} = 0$. It turns out that the direct numerical implementation of this simple idea is a complicated issue (see the discussion of the null-space problem later in this section).

Any set of $F_j(x; k)$ which are solutions of the Helmholtz equation may be used for the DEM. However, it should be remembered that computationally not all bases are equivalent. For instance, the Y_0 basis defined by equation (3), which might appear to be the best choice as a DEM basis due to its association with the BIM, does not give the best numerical results when compared against other options. In particular, it turns out that the PWDM is typically much more effective (recall that the PWDM is a special case of the DEM, corresponding to the choice (2) of basis functions). Finally we note that the set of J_0 of equation (4) cannot be regarded as a mathematically legitimate basis for a DEM. This latter point will be explained in section 5.

For the Y_0 basis the BIM and the DEM lead to the same equation. It is only the mathematical interpretation that is different. Within the DEM, one regards the Y_0 as basis functions to be used in an expansion, while the same Y_0 in the BIM context serves as the Green function. In the context of DEM, one may be bothered by the singular nature of the Y_0 functions: the constructed wavefunction should be zero on the boundary. Mathematically this is achieved in the $N \to \infty$ limit, so the Y_0 basis is a valid choice. But in an actual numerical implementation, the wavefunction so constructed will always have singularities on the boundary. One possible remedy consists of enforcing the boundary conditions on intermediate boundary points, or on points that lie on an outer boundary. Alternatively, one may replace the bare Y_0 basis by smooth superpositions of Y_0 functions (see appendix C).

In figure 2, we show an example of a numerically determined C (using the PWDM basis) for one of the pond eigenstates, while in figure 3 we illustrate the constructed wavefunction. Unlike the Green function construction, the DEM/PWDM constructed wavefunction does not vanish outside the boundary. Actually, it is quite the opposite: typically the DEM/PWDM wavefunction becomes exponentially large as we go further away from the boundary. Whenever this behaviour occurs, it constitutes an indication of the *evanescent* nature of

the wavefunction. Namely, in such cases, the wavefunction acquires sub-wavelength features in order to accommodate the boundary. This requires exponential behaviour (negative kinetic energy) in the transverse space direction, in order to keep the total energy fixed.

3.3. Normalization of the wavefunction

A standard SVD procedure generates vectors Φ_s and C_j that are normalized in the sense $\sum_s |\Phi_s|^2 = 1$ and $\sum_j |C_j|^2 = 1$. Therefore, the constructed Ψ_r is not properly normalized within the interior region. Adopting the usual philosophy of boundary methods, the problem of calculating the Ψ_r normalization is reduced to that of evaluating a boundary integral, namely [8, 18]

$$\int\int |\Psi(x)|^2 \, dx = \frac{1}{2k^2} \oint |\Phi(s)|^2 (n(s) \cdot x(s)) \, ds. \tag{15}$$

For the BIM, by discretizing equation (15) we obtain the following numerical expression for the normalization factor:

$$\|\Psi_r\| = \frac{1}{\Delta s} \sum_s \mathbf{w}_s (\Phi_s)^2 = \Phi^\dagger \mathbf{W} \Phi. \tag{16}$$

Here $\mathbf{W} = (1/\Delta s) \, \mathrm{diag}(\mathbf{w}_s)$ is a diagonal matrix, and the weight factor $\mathbf{w}_s$ is defined in table 1. As for the DEM, by using the derivative of equation (14) in equation (11) and substituting into equation (15), we get

$$\|\Psi_r\| = \Delta s \sum_s \mathbf{w}_s \left(\sum_j C_j \mathbf{D}_{js} \right)^2 \tag{17}$$

$$= \sum_{ij} C_i \mathbf{B}_{ij} C_j = \mathbf{C} \mathbf{B} \mathbf{C}^\dagger. \tag{18}$$

The definitions of D_{js} and of the metric B_{ij} can be found in table 1.

The normalization $\|\Psi_r\|$ can be calculated using the metric $\mathbf{B}_{ij}$. This method looks quite elegant, but it does not turn out to be very effective numerically. Consider equation (17). This equation is quite safe computationally for two reasons: (i) all its terms are non-negative; (ii) standard summation routines order these terms in descending order. Now, let us look instead at equation (18). In this case the numerical calculation can give *any* result (if we go to large k). Sometimes, the answer even comes out to be negative! This occurs because the calculation involves many arbitrarily ordered terms that each has a different algebraic sign.

3.4. The tension along the boundary

The numerical wavefunction Ψ_r satisfies the Helmholtz equation in the interior region *by construction*. Thus, whether Ψ_r is an actual eigenstate depends on its behaviour along the boundary. In this subsection we discuss the definition of a 'tension' measure that estimates whether, and to what accuracy, the numerical Ψ_r satisfies the boundary conditions.

For the case of the DEM, following [9], the tension is defined as the boundary integral

$$\|\Psi_s\| = \Delta s \sum_s \left(\sum_j C_j \mathbf{A}_{js} \right)^2 = \sum_{ij} C_i \mathbf{T}_{ij} C_j = \mathbf{C} \mathbf{T} \mathbf{C}^\dagger. \tag{19}$$

The standard practice to date for the tension calculation has been to use a denser set of boundary points located between the x_s points. However, our experience (see also [5]) is that the tension
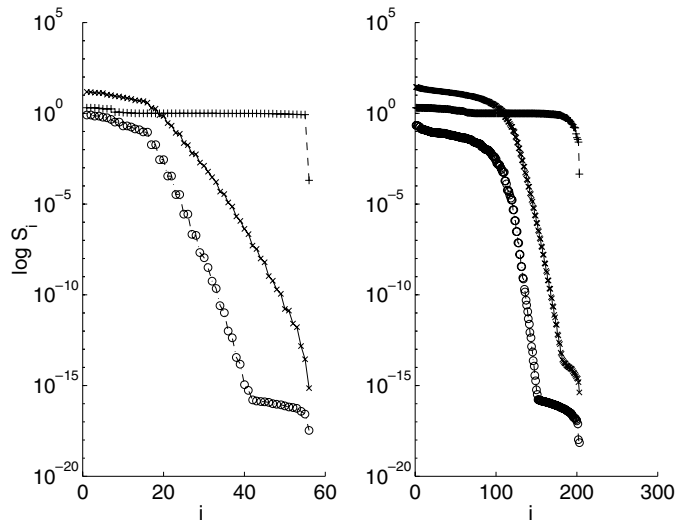
Figure 4. Singular values of the Fredholm matrix for $k_n = 6.827\,545\,928\,676\,94$ (left plot) and for $k_n = 50.054\,749\,120\,044\,08$ (right plot). The various symbols are as in figure 2.

estimate obtained from the initial set of points is just as effective. This is demonstrated in figure 3(d). Therefore, we routinely rely on the same set of boundary points to determine the tension.

For the BIM on the other hand, the above definition is not practical due to the singular nature of the basis functions. For any finite M, the numerical wavefunction blows up at each boundary point. However, since the BIM wavefunction vanishes everywhere outside the billiard, a numerically unambiguous definition of tension arises as an integral of $|\Psi(x)|^2$ along an outer boundary:

$$\|\Psi_s\| = \Delta s \sum_s (\Psi_s)^2 = \Delta s \sum_s \left(\sum_s \mathbf{G}_{ss} \Phi_s \right)^2. \tag{20}$$

By outer boundary (see figure 1), we mean the set of external points (s points, as opposed to s points for the true boundary) that have a fixed transverse distance ΔL from the true boundary. The distance ΔL between the boundary and the outer boundary should be small on any classical scale but large compared with ds, in order for the tension to be independent of the choice of ΔL. See figure 5(c) for a numerical demonstration.

3.5. The PWDM and the null-space problem

One may think that C could be found simply by computing the (left) eigenvector that corresponds to the smallest singular value of $\mathbf{A}_{js}$. Numerically this definition is hard to implement. This difficulty can be explained by looking at the behaviour of the singular values of $\mathbf{A}_{js}$ for the PWDM basis. Figure 4 gives some examples of singular values resulting from the SVD of the $\mathbf{A}_{js}$ matrix. In the case of the PWDM, as k become large, one observes that the singular values separate into two groups: rather than having one distinctly smaller singular value, we obtain a whole set of them. Accordingly, we can define a numerical 'null space' of the $\mathbf{A}_{js}$ matrix.

The interpretation of this null space is quite clear. It is well known [19, 20] that it is not efficient to include much more than N_{sc} plane waves in the basis set $F_j(x; k)$, where

$$N_{sc} = \frac{1}{\pi} kL \tag{21}$$

and L is the perimeter of the billiard. The reason for this ineffectiveness is that k_i and k_j cannot be distinguished numerically within the interior region unless $|k_i - k_j|L > 1$. In order to obtain the semiclassical result (21), the total phase space area ($L \times (2mv)$) of the boundary Poincaré section is divided by the size of the Planck cell ($2\pi\hbar$). If we use $N > N_{sc}$ plane waves, then we can create *wavefunctions that are nearly zero in the interior*, and become large only as we go far away from the centre [21]. It is clear that the SVD can be used to determine the $N - N_{sc}$ null space of these evanescent states. Whenever k is an eigenvalue, this null space includes, in addition to the evanescent waves, the single eigenvector that constitutes an eigenstate of the Helmholtz equation. The problem is to distinguish this eigenvector from the other vectors in the null space.

The basic difference between the eigenvector that leads to an eigenstate (which exists if $k = k_n$), and the other vectors in the null space is related to the normalization. As discussed before, a standard SVD procedure generates vectors C_j that are normalized in the sense $\sum_j |C_j|^2 = 1$. Therefore, the Ψ_r of equation (6) is not properly normalized within the interior region. Normalizing the wavefunction has the effect of magnifying the evanescent solutions in the interior as well as on the boundary, while the eigenfunction (if it exists) remains small on the boundary. In appendix D, we give a detailed explanation of the numerical procedure for finding C_j that can be derived from the above observation.

4. The quantization measure

Once we have constructed the wavefunction at a given k, the next step is to determine whether Ψ is an eigenstate. As we will explain below, our choice of measures reduces to finding the minima of one of

$$S(k) = \text{tension} \tag{22}$$

$$S(k) = \text{smallest singular value} \tag{23}$$

$$S(k) = \text{determinant.} \tag{24}$$

We call $S(k)$ the quantization measure. Below we give further explanation of the above definitions.

It is clear that the most natural quantization measure is the tension. If a properly normalized wavefunction has 'zero tension' on the boundary, it means that the corresponding k is an eigenvalue. The normalization issue is further discussed in appendix D. The question that arises is whether we can use a numerically simpler measure, and what price we pay for doing so.

The BIM equation (12) and the GFM equation (13) can both be written as $A\Phi = 0$, with the appropriate choice of A. Thus, if k is an eigenvalue, A should have a singular value that tends to 0 as N increases. The determinant of A is defined as the product of all the singular values, and therefore it should vanish whenever one of the singular values does. Using the *GFM–DEM duality* which is discussed in section 5, it is clear that for the DEM (and for the PWDM in particular) the determinant of A vanishes whenever k is an eigenvalue. It is important to realize that in the latter argumentation, *we do not rely on inside–outside duality* [20] considerations, but rather on the much simpler *GFM–DEM duality*.

Thus, a low tension must be correlated with having a vanishingly small singular value or determinant. The converse is not true: it is well known that SVD based quantization measures may lead to spurious minima (see [4] and references therein). Therefore the SVD based procedure for finding eigenvalues requires a post-selection procedure whose aim is to distinguish true zeros from fake ones.

It is important to realize that neither the traditional implementation of PWDM, nor that of the BIM should be considered to be 'package deals'. For example, the BIM could be used with the tension as a measure (defined in the next section), rather than looking for minima of the singular values. Similarly, the usual Heller method of PWDM implementation (see appendix D) could be replaced by a search over determinant values.

4.1. The tension as a quantization measure

The tension is a robust measure of quantization. Figure 5 shows some examples of the corresponding $S(k)$ plots. The PWDM minima are typically much sharper than their BIM equivalents. Zooming over a PWDM minimum (figure 5(d)) reveals some amount of roughness. This feature is actually helpful, because it gives an indication of and control over the accuracy of the numerics. We interpret the roughness of the PWDM minimum as a reflection of the existence of a null space. In the same spirit, the smoothness of the BIM minima can be regarded as an indication that better accuracy can be obtained by making N larger. We discuss these issues below.

The tension provides a common measure that may be used to monitor improvements, as well as to compare the success of the different methods. Naturally, the first issue to discuss is the dependence of the tension on the size N of the basis set (see figure 6). For the BIM, the tension becomes better as N increases, and disregarding the computer hardware, there is no reason to suspect that there is an inherent limitation on the accuracy. The situation is different for the PWDM. Here, taking N much larger than N_{sc} is not effective. In practice, the method reaches a limiting accuracy, which, taking into account present hardware limitations, is still very good compared with that of the BIM.

From figure 6, it is also clear that the tension of the PWDM becomes much better as k becomes larger. This is expected on the basis of the following semiclassical reasoning: larger uncertainties in k result from confining a particle to a smaller box (taking a smaller box for a given k is equivalent to making k smaller for a given box size). Thus, it is more difficult to build a wavefunction with a precise value of $|k_j| = k$ for low-lying eigenstates. On the other hand, the BIM does not seem to be sensitive to the value of k.

4.2. The tension as an indication for the global error

The tension can be regarded as a measure of the *local error* in the determination of the eigenfunction. The tension is local in the sense that it pertains only to points along the boundary. We can also define a measure for the *global error*, that is the error which is associated with all the interior points:

$$(\Delta\Psi)^2 = \langle|\Psi_r - \Psi_{exact}(X_r)|^2\rangle. \tag{25}$$

Here $\Psi_{exact}(x)$ is the numerically exact wavefunction. The average is taken over the set X_r of selected points inside the boundary. Figure 7 shows an example of the variation of the error along the cross-section line of figure 1. In order to eliminate a possible bias due to a global normalization error, we renormalized the inexact wavefunction so that $\Psi_r = \Psi_{exact}(X_r)$ at a randomly selected point $X = X_0$. In retrospect, we realized that such an error did not

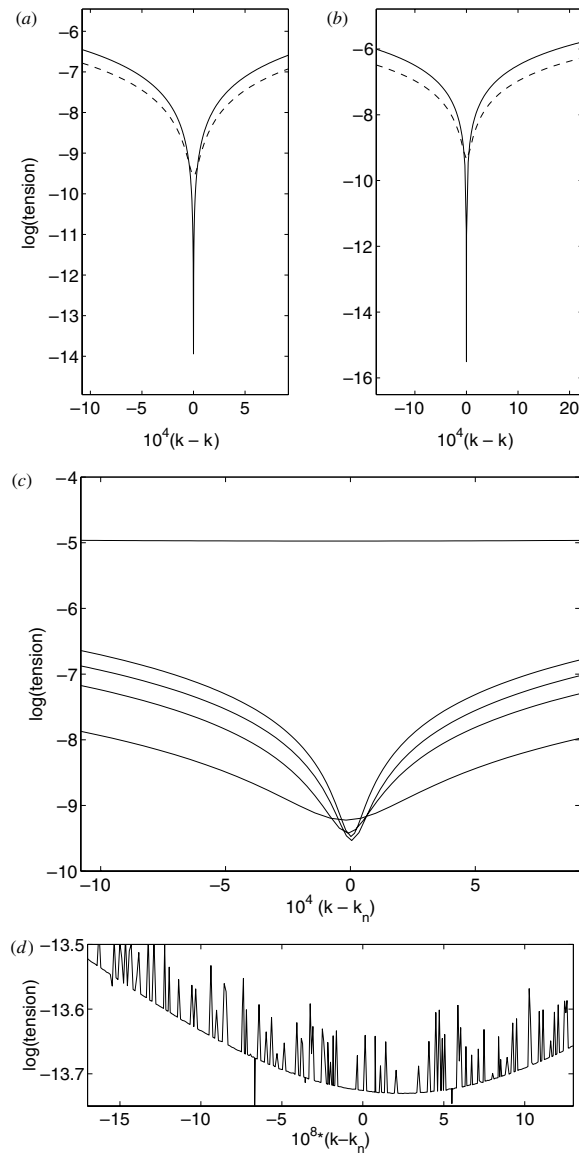**Figure 5.** The tension as a function of k in the vicinity of $k_n = 10.147\,079\,715\,172\,64$ (panels (a), (c) and (d)), and of $k_n = 50.054\,749\,120\,044\,08$ (panel (b)). In the upper panels ((a) and (b)) the full line is for the PWDM constructed wavefunction, while the dashed line is for the BIM constructed wavefunction. For the low-k state we chose $b = 4$, while for the high k we used $b = 2$. Panel (c) demonstrates the dependence of the BIM tension on the choice of the distance ΔL. The different curves (from the upper to lower) correspond to $\Delta L/\Delta s = 1, 8, 16, 12, 4$. Panel ($d$) is a zoom over the PWDM minimum.

significantly affect the result. However, we still chose to be on the safe side, and we adopted this procedure routinely.

It is natural to expect the average error $(\Delta \Psi)^2$ to be correlated with the tension. In other words, if $|\Psi_r - \Psi_{\text{exact}}(X_r)|$ is small on the boundary, then one may expect it to be small in the interior. The degree of such correlation is important for practical reasons. Moreover, we
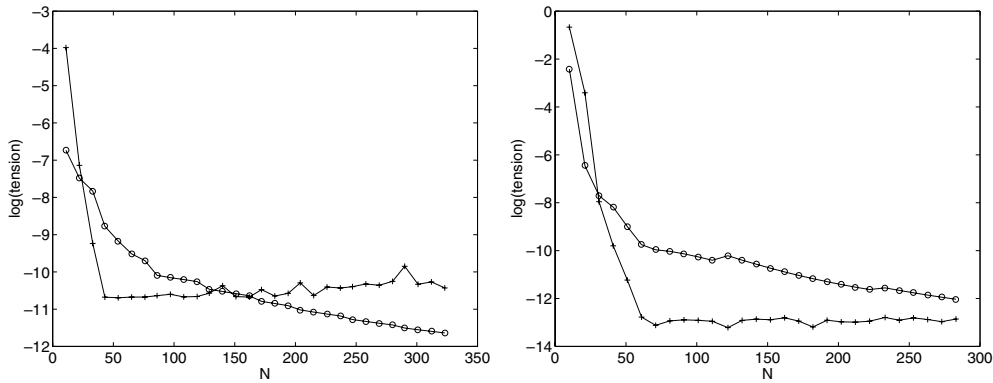
Figure 6. The tension for the constructed eigenstate versus the number N of basis functions. The left plot is for the $k_n = 2.404\,256\,577\,923\,91$ eigenstate, and the right plot is for the $k_n = 6.827\,545\,928\,676\,94$ eigenstate. The symbols ($\circ$) and (+) are for the BIM and for the PWDM, respectively.
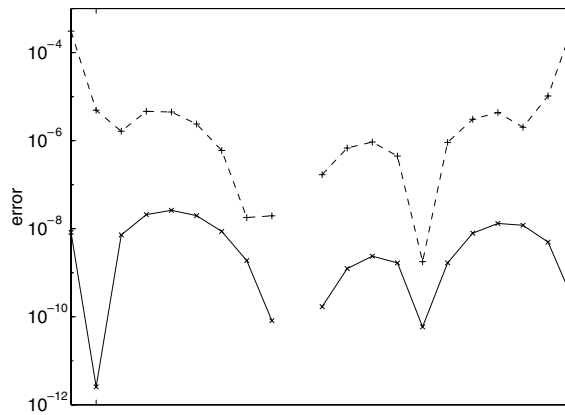

Figure 7. Plot of the error $|\Psi_r - \Psi_{\text{exact}}(X_r)|^2$, along the cross-section line of figure 1. We refer here to the $k_n = 6.827\,545\,928\,676\,94$ eigenfunction. The numerically 'exact' wavefunction is our best PWDM constructed wavefunction ($N = 69$) with tension $= 10^{-13}$. The 'non-exact' wavefunction is either BIM constructed (+) or PWDM constructed ($\times$), with tension $\approx 10^{-8}$. In the middle point the error is zero by construction (see explanation in the text).

have introduced two different versions of tension definitions, one for each of the PWDM and the BIM. It is not *a priori* clear that the above correlation is independent of the choice of the numerical method. In figure 8, we study this issue by plotting $(\Delta\Psi)^2$ against the tension for the BIM and the PWDM. In the case of the PWDM, the error saturates below a critical tension. After this point, further improvements on the boundary do not seem to affect the bulk of the eigenstate. It is not clear from the numerics whether or not the BIM saturates. What is clear however is that the BIM does a poorer job at reproducing the wavefunction inside the boundary than the PWDM with the same tension.

The saturation of the error well inside the billiard can be explained as a manifestation of the fact that the wavefunction there is not very sensitive to the sub-wavelength roughness of the boundary: if N is reasonably large, the numerical wavefunction vanishes on a nodal line
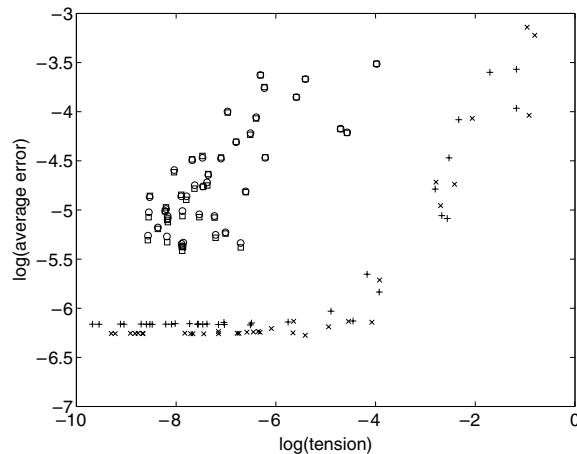
Figure 8. The average error in the determination of the wavefunction, versus the tension for the $k_n = 6.827\,545\,928\,676\,94$ eigenfunction. For the BIM constructed wavefunction we use squares and ($\circ$), while for the PWDM one we use ($+$) and ($\times$). The error has been determined with respect to the 'exact' wavefunction Ψ_{exact}. The latter is numerically defined as either the best BIM eigenstate (squares and ($+$)) or as the best PWDM one (($\circ$) and ($\times$)). For both choices Ψ_{exact} had a tension better than 10^{-10}.

that almost coincides with the true (predefined) boundary. Increasing N further affects the sub-wavelength features of the (distance) difference between that nodal line and the true boundary. This distance difference is important for the tension, but barely affects the wavefunction well inside the billiard.

4.3. The determinant as a quantization measure

The tension is the natural choice for a quantization measure. However, from a numerical point of view, it is much more convenient and time effective to compute the singular values of **A**, without having to find the eigenvectors for each k value, and without having to compute the wavefunction along the boundary (for tension calculation).

The smallest singular value is traditionally used as a quantization measure for the BIM. From figure 7, it is quite clear that for the BIM one of the singular values is significantly smaller than the others, so that the eigenstate is unambiguously determined by this method. Is it possible to use the same approach, with comparable success, for the PWDM? We have already determined that looking at the smallest singular values is not very meaningful numerically. For $N > N_{\text{sc}}$, there exists a large null space of evanescent states for any k. The metric method (appendix D) is not a practical solution to this problem since we want to gain numerical efficiency (if efficiency is not the issue then it is better to use the tension as a quantization measure).

One simple way to improve the numerical stability is to use the determinant rather than the smallest singular value as a quantization measure: each time that $k = k_n$, the null space should include one more 'dimension'. Therefore, the determinant, rather than the smallest singular value, becomes the reasonable quantity to look at. Thus, from the numerical point of view (23) should be superior compared with (22).

Figure 9 illustrates how the determinant can be used in practice as a quantization measure. As a general rule, as is the case for the tension, the PWDM/GFM minima are sharper than the
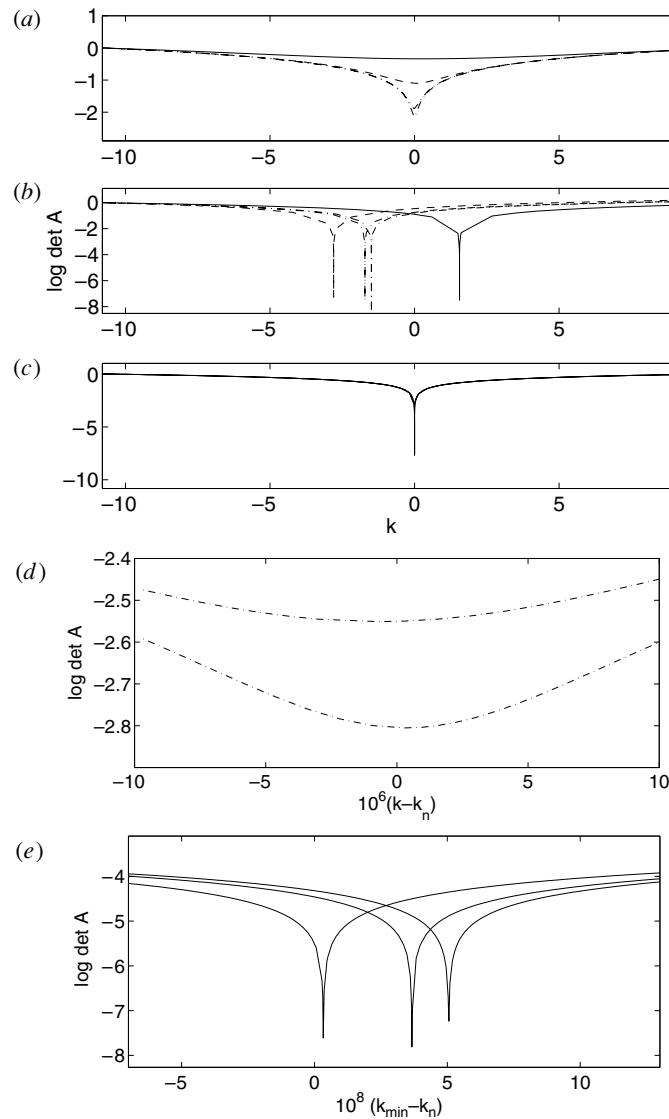
Figure 9. The Fredholm determinant ($S(k)$) versus k in the vicinity of $k_n = 10.147\,079\,715\,172\,64$. Note that $S(k)$ is normalized such that $S(k) = 1$ away from the minima. Panels (a)–(c) show $S(k)$ in the cases of the H1-BIM, the Y1-BIM and the PWDM, respectively. The lines plotted, in the order of decreasing $S(k)$ minimum, correspond to $b = 2, 3, 4, 8$ in panel (a), $b = 4, 8, 13, 12$ in panel (b) and $b = 2$ in panel (c). The PWDM run in panel (c) was repeated three times with different values of the randomly chosen plane-wave phases. Panels (d) and (e) give a zoom over the minima of panels (a) and (c), respectively. We witness some numerical instabilities for both the Y1-BIM and the PWDM, though in the latter case it is much much weaker, and can be resolved only in the zoomed plot (panel (e)). For larger b values, the PWDM instability is enhanced, and the results are reduced to numerical garbage (not shown).

BIM ones. On the one hand, this extra sharpness can be regarded as an advantage, because it leads to a better resolution of the eigenvalue spectrum. However, more computer time is

needed in order to find these minima. The BIM minima are broader, and therefore digging algorithms that search for local minima become extremely effective.

In the case of the traditional BIM, using a larger N leads to a better resolution of the local minima, as expected. The traditional H-BIM uses the complex Hankel–Bessel function as its Green function. One may wonder why the real Neumann function could not be used instead. *A priori*, there is no reason to insist on Hankel choice. However, it seems that with Neumann choice the numerics are not very stable: the locations of the local minima vary on a k range which is large compared to their k width. Because of this problem, search routines relying on the Y-BIM may yield misleading values for the error in the k_n determination. Thus, the numerical stability of the H-BIM can be attributed to the fact that the BIM equation $\mathbf{A}\Phi = 0$ becomes complex. Its real part is just the Y-BIM equation, while its imaginary part is the J-GFM equation. Thus one may say that the H-BIM benefits from combining the Y-BIM with the J-GFM.

Is it practical to use the Fredholm determinant as a quantization measure also in the GFM/PWDM case? Here we observe that the null-space problem is reflected in the stability of the determinant calculation. It is useful to characterize the numerics using the discretization parameter b:

$$b = \frac{N}{N_{sc}} = \left.\frac{\lambda/2}{\Delta s}\right|_{M=N}. \tag{26}$$

The last equality holds if we take $M = N$, leading to the interpretation of b as the number of boundary points per half de Broglie wavelength. If $b < 1$ the null-space problem does not exist, and we can define C as the (left) eigenvector that corresponds to the smallest singular value of $\mathbf{A}_{js}$. Of course, we want to push PWDM to the limit, and therefore in practice we always take $b > 1$.

The natural question is whether choosing a very large b is numerically useful. Our numerical experience is that for $1 < b < 1.8$ we get nice minima, which actually look much sharper than the BIM ones (see figure 9). As we try to increase b in order to improve accuracy, the numerics lose stability (what we mean by instability is demonstrated in figure 9(e)). The same phenomenon occurs with J0-GFM, which has a somewhat larger tendency for instability. This is apparently because the J0-GFM is involved with a larger null space (see figure 4).

Thus we conclude that taking $b > 1$ does improve the numerics, while $b \gg 1$ generally leads to instabilities that should be avoided. The optimal choice of b depends on the details of the implementation and on the computer hardware. It should be clear that if the numerical accuracy were unlimited, then the $b \to \infty$ limit would lead to a numerically exact solution in cases where the wavefunctions may be written as superpositions of plane waves. This is not always possible [17]. Note however that evanescent features of the wavefunction can be reconstructed by a suitable superposition of plane waves [21].

5. The duality of the GFM and the DEM

In addition to providing a boundary method of its own, the GFM also serves to bridge the gap between the BIM and the DEM. Consider the version of the GFM that is based on the choice $\mathcal{C}(x, x') = F_j(x; k)$, where the F_j are solutions of the Helmholtz equation in free space (with neither singularities nor cuts). With this choice, we immediately realize that the DEM and the GFM are dual methods:

$$\mathbf{A}\Phi = 0 \qquad \text{(GFM equation)} \tag{27}$$

$$\mathbf{C}\mathbf{A} = 0 \qquad \text{(DEM equation)}. \tag{28}$$

The only difference lies in whether one looks for the *left* or the *right* eigenvector. This point is numerically demonstrated in figure 2.

The PWDM version of the DEM also satisfies this duality. In this special case, a somewhat more elegant version of the above argument is as follows. Consider the version of the GFM that is based on the choice $\mathcal{C}(x, x') = \exp(\mathrm{i}k n_j \cdot (x - x'))$, where n_j is a unit vector in a given direction. We can take N different choices of n_j, thus obtaining the matrix equation $\mathbf{A}\Phi = 0$ with

$$\mathbf{A}_{js} = \exp(\mathrm{i}k n_j \cdot x_s). \tag{29}$$

An equivalent matrix equation is found by multiplying each equation by $\exp(\mathrm{i}k\phi_j)$, where ϕ_j are random phases. We can then take the real part of these equations, thus obtaining a set of equations that involves the same matrix $\mathbf{A}$ as that of PWDM, namely (5) with the basis defined by (2).

The duality of the PWDM and the GFM is very important from a mathematical point of view. The mathematical foundations of the PWDM are quite shaky. It is clear that PWDM is well established mathematically if a strict 'inside–outside duality' (IOD) [20] is satisfied. In this case, the wavefunction can be extended to the whole plane so that the boundary of the billiard can be regarded as a *nodal line* of some plane-wave superposition. Obviously, this is rarely possible [21]. Therefore, one may wonder whether we indeed have $\det(\mathbf{A}) = 0$ whenever $k = k_n$. Using the duality (27), it becomes obvious that the Fredholm determinant indeed vanishes at the eigenstates, even in the absence of an exact IOD.

It is quite clear from the first paragraph of this section that any expansion method can be associated with a corresponding GFM. Whenever the left eigenvector is used with the expansion method, the right eigenvector can be used with the GFM. We have already demonstrated this point in figure 2. Is it possible to make the inverse statement? Do we have a well-defined expansion method associated with any GFM? The answer is negative. We discuss this issue in the rest of this section, and it can be skipped at first reading.

For the following, it is convenient to consider equation (6) as $N \to \infty$. Subsequently, we are going to talk about whether this limit is meaningful. In the case of the usual PWDM, the $N \to \infty$ limit of equation (6) can be written as

$$\Psi(x) = \int_0^{2\pi} \mathsf{C}(\theta)\, \mathrm{d}\theta \, \exp(\mathrm{i}k n(\theta) \cdot x). \tag{30}$$

Similarly, in the case of the J_0 decomposition, using the basis functions of equation (4), we can write by complete analogy

$$\Psi(x) = \oint \Phi(s)\, \mathrm{d}s\, J_0(k|x - x(s)|). \tag{31}$$

In writing equation (31) we have used the fact that $J_0(x(j) - x(s))$ is a symmetric kernel, and therefore we could make the substitution $\mathsf{C} = \Phi$. Equation (31) looks at first sight like an innocent variation of equation (30). The Bessel function J_0 is just a superposition of plane waves, and therefore one may possess the (incorrect) idea that there is a simple way to go from equation (31) to equation (30). If we expand each J_0 in equation (31) in plane waves, and rearrange the expression in order to identify the PWDM coefficients, we end up with the relation

$$\mathsf{C}(\theta) = \int \mathrm{e}^{-\mathrm{i}k n(\theta) \cdot x(s)} \Phi(s)\, \mathrm{d}s. \tag{32}$$

This relation implies the trivial result $\mathsf{C}(\theta) = 0$ due to gauge freedom (see the discussion of equation (29)). Hence we conclude that the constructed wavefunction is $\Psi(x) \equiv 0$ in the $N \to \infty$ limit!

Having $\Psi(x) \equiv 0$ from equation (31) could have been anticipated using a simpler argument. We know that equation (10) should hold for *any* gauge choice. This gauge freedom implies that we have

$$\oint \mathcal{C}(x, x(s)) \Phi(s) \, \mathrm{d}s = 0. \tag{33}$$

The above equation should hold for any x inside as well as on the boundary. Furthermore, the left-hand side of (33) is manifestly a solution of Helmholtz equation in free space, and it follows from the unique continuation property that equation (33) holds also for points outside the boundary. Having $\Psi(x) = 0$ as a result of the integration in equation (31) is just a particular case of equation (33).

In spite of the observation that equation (31) yields $\Psi(x) \equiv 0$ in the $N \to \infty$ limit, the vector Ψ_r is non-zero numerically for any finite N. In fact, after proper renormalization, Ψ_r becomes a quite good approximation to the wavefunction (see figures 3(*c*) and (*e*)). Sometimes the result so obtained is even better than the one which is found via the traditional BIM equation (7). As strange as it sounds, this success is entirely due to the fact that we are using finite N.

6. Conclusion

The BIM and the DEM were written as different faces of a unified boundary procedure comprising four steps. In the process of doing so, yet a third boundary method was derived as part of the same framework, the GFM. The DEM and the GFM are strongly related, as they are respectively the left and the right eigenvectors of the same Fredholm matrix. We think that the presented approach opens the way towards a controlled fusion of the BIM and the DEM into a more powerful numerical procedure.

The unified treatment of quantization measures allowed us to compare the efficiency of the various methods, and to analyse both the local and the global errors in the numerically determined wavefunction. In particular, a numerically valid definition of the BIM tension was given, and was found to possess smooth minima at the eigenstates. Using the tension as a quantization measure is one possible way to avoid some problems [4] that are encountered in the traditional implementation of the BIM.

Acknowledgments

Appendix A. The BIM for the scattering problem

The solution of the Helmholtz equation for the scattering problem is just another variation of the BIM. Consider a boundary, one that in general may be composed of several disconnected pieces. The incident wave $\Psi_{\text{incident}}(x)$ is a solution of Helmholtz equation in free space. Formally, $\Psi_{\text{incident}}(x)$ includes both the ingoing and the outgoing wave components. We look for a solution $\Psi(x)$ that has the same ingoing component as $\Psi_{\text{incident}}(x)$, and that satisfies

$\Psi(x) = 0$ on the boundary. Such a solution can be written as a sum of the incident wave and a scattered wave, and hence must be of the form

$$\Psi(x) = \Psi_{\text{incident}}(x) + \oint G(x, x(s'))\Phi(s') \, ds. \tag{A.1}$$

Equation (A.1) is a variation of equation (10). Note that the Green function should satisfy outgoing boundary conditions in order to yield the desired solution. The charge density $\Phi(s)$ is fixed by the requirement that $\Psi(x) = 0$, which leads to the boundary equation

$$\oint G(x(s), x(s'))\Phi(s') \, ds = -\Psi_{\text{incident}}(s). \tag{A.2}$$

This inhomogeneous equation is a straightforward generalization of equation (12). A discretized version of it was used in [22] in order to obtain numerical solutions of the Helmholtz equation for some scattering problems.

The derivation of equation (A.2) in [22] is much more complicated than ours, and involves the use of the Lippmann–Schwinger equation. The boundary is represented by a large delta potential V, and the limit $V \to \infty$ is taken. Using this procedure, the charge density $\Phi(s)$ can be obtained as the $V \to \infty$ limit of $V\Psi(x(s))$. Note the correctness of the physical units. Namely, $[\mathcal{H}][\Psi] = [\rho]$ and therefore $[V][\Psi] = [\Phi]$. Note also that the wavefunction is in general non-zero in both sides of the boundary. Therefore the charge density $\Phi(s)$ is equal to the *difference* between the normal derivatives on both sides of the boundary. The simplest way to derive the relation between $\Phi(s)$ and $V\Psi(x(s))$ is to integrate the Helmholtz equation over an infinitesimal range across the boundary, as in the treatment of the 1D Schrödinger equation with delta potential.

Appendix B. Traditional BIM equation

The primitive BIM equation (equation (12)) is based on equation (10). The traditional BIM is a variation of the same idea which avoids the boundary singularities that plague the more simplistic version. Rather than using equation (10) directly, one considers its gradient, leading to

$$\partial_{\pm}\Psi(x(s)) = \oint \partial_{\pm}G(x(s), x(s'))\Phi(s') \, ds'. \tag{B.1}$$

This equation is analogous to equation (12). We use the notation ∂_+ and ∂_- in order to refer to the normal derivative on the interior and exterior sides of the boundary. By definition, $\partial_-\Psi(x(s)) = \Phi(s)$, and from the discussion in section 3 we have $\partial_+\Psi(x(s)) = 0$. Adding the two equations of (B.1), we obtain

$$\Phi(x(s)) = \oint 2\partial G(x(s), x(s'))\Phi(s') \, ds' \tag{B.2}$$

where $\partial \equiv (\partial_+ + \partial_-)/2$ is just the derivative on the boundary in the principal sense. Thus, in the traditional BIM, the definition of the Fredholm matrix is

$$\mathbf{A}_{ss'} = \frac{1}{\Delta s}\delta_{ss'} - 2\partial G(x(s), x(s')) \tag{B.3}$$

and the BIM equation (B.2) is $\mathbf{A}\Phi = 0$. The kernel $\partial G(x(s), x(s'))$ is well behaved, and its diagonal elements are finite thanks to the presence of a geometrical factor. Namely, if $G(x(s), x(s')) = g(k|x(s) - x(s')|)$ then

$$\partial G = k\frac{n(s) \cdot (x(s) - x(s'))}{|x(s) - x(s')|} g'(k|x(s) - x(s')|). \tag{B.4}$$

If either one of the Bessel functions H_0 or Y_0 is used for the Green function, then the definition of $\mathbf{A}_{ss'}$ above involves either H_1 or Y_1, respectively.

Appendix C. Transformed BIM equations

There exists another elegant version of the BIM [14–16] which does not exhibit the singularities associated with the Y0-BIM. Namely, the BIM equation is rewritten as

$$\int \tilde{G}(x(j), \kappa) \tilde{\Phi}(\kappa)\, d\kappa = 0 \tag{C.1}$$

where the vector $\tilde{\Phi}(\kappa)$ is related by a linear transformation to the vector $\Phi(s)$. This transformation corresponds to the selection of a complete basis set of boundary wavefunctions. The KKR method [16] is a particular implementation which uses the spherical harmonics. Another (more general) choice [14, 15] consists of taking $\tilde{\Phi}(\kappa)$ as the Fourier components of $\Phi(s)$. In the latter case $\tilde{G}$ is related to G by the Fourier transform $s \mapsto \kappa$. However, obtaining $\tilde{G}$ from G is not simple for most boundary shapes.

Appendix D. The PWDM, in practice

The mathematically clean solution for the null-space problem is to adopt a method based on a metric. As we explain in the next paragraph, this procedure is sensitive to cumulative numerical errors. A modified implementation of the metric method, which avoids some of the numerical problems, has been introduced by Barnett [5]. The other possibility is to use a very simple procedure which is known as Heller's method [9]. Below we discuss the latter as well.

The metric method works as follows. First, one finds the basis in which the normalization metric $\mathbf{B}_{ij}$ becomes δ_{ij}. The tension metric $\mathbf{T}_{ij}$ should then be written in that same basis. The SVD is done on the transformed tension metric. In this case, the null space becomes at most one dimensional (whenever $k = k_n$). Unfortunately, this elegant and straightforward metric scheme does not work very well, due to the finite precision problems discussed in connection with equation (18). Furthermore, $\mathbf{B}$ and $\mathbf{T}$ are 'squares' of $\mathbf{A}$, which leads to a loss of numerical precision compared with an $\mathbf{A}$-based strategy.

The most widely used $\mathbf{A}$-based strategy is referred to as Heller's method [9]. The idea is to find C_j as the solution of the $M \geqslant N$ set of equations $\sum_j \mathsf{C}_j \mathbf{A}_{js} = 0$, with the additional constraint $\sum_j \mathsf{C}_j \mathbf{A}_{j0} = 1$. Table 1 gives the definition of $\mathbf{A}_{j0}$.

By constraining the wavefunction to be $\Psi(X_0) = 1$ at a selected point X_0 in the interior of the billiard, we eliminate the problems associated with evanescent states, as the associated (evanescent) wavefunctions no longer vanish on the boundary and thus, there is no longer a null-space problem. As a result, quite large b can be used without encountering numerical instabilities. The only worry with this method is that X_0 may happen to be very close to a nodal line. In such cases, the tension will be large due to an improper normalization, so we will miss these eigenstates.

References

[1] Stockmann H J 1999 *Quantum Chaos: An Introduction* (Cambridge: Cambridge University Press)
[2] Datta S 1997 *Electronic Transport in Mesoscopic Systems* (Cambridge: Cambridge University Press)
[3] Kuttler J R and Sigillito V G 1984 Eigenvalues of the Laplacian *SIAM Rev.* **26** 163–93
[4] Backer A 2003 *The Mathematical Aspects of Quantum Maps* ed M Degli Esposti and S Graffi (Berlin: Springer) (*Preprint* nlin.CD/0204061)

[5] Barnett A 2000 *PhD Thesis* Harvard University
[6] Robnik M 1983 *J. Phys. A: Math. Gen.* **17** 1049
[7] Luna-Acosta G A, Kyungsun Na and Reichl L E 1996 *Phys. Rev.* E **53** 3271
[8] Berry M V and Wilkinson M 1984 *Proc. R. Soc. Lond.* A **392** 15
    Kleinman R E and Roach G F 1974 *SIAM Rev.* **16** 214–36
    Riddell R J 1979 *J. Comput. Phys.* **31** 21
    McDonald S W and Kaufman A N 1988 *Phys. Rev.* A **37** 3067–86
[9] Heller E J 1991 *Chaos and Quantum Systems* ed M-J Giannoni, A Voros and J Zinn-Justin (Amsterdam: Elsevier) p 548
[10] Vergini E 1995 *PhD Thesis* Universidad de Buenos Aires
[11] Vergini E and Saraceno M 1995 *Phys. Rev.* E **52** 2204
[12] Li B, Robnik M and Hu B 1998 *Phys. Rev.* E **57** 4095
[13] Lepore N, Cohen D and Heller E J in preparation
[14] Hornberger K and Smilansky U 2000 *J. Phys. A: Math. Gen.* **33** 2829
[15] Hornberger K 2001 Spectral properties of magnetic edge states *Dissertation* Ludwig-Maximilians-Universitat, Munchen, Online at http://www.mpipks-dresden.mpg.de/klh/pubs
[16] Berry M V 1981 *Ann. Phys.* **131** 163–216
[17] Gutkin B 2003 *Preprint* nlin.CD/0301031
[18] Boasman P A 1994 *Nonlinearity* **7** 485
[19] Dietz B and Smilansky U 1993 *Chaos* **3** 581
[20] Dietz B *et al* 1995 *Phys. Rev.* E **51** 4222
[21] Berry M V 1994 *J. Phys. A: Math. Gen.* **27** L391
[22] da Luz M G E, Lupu Sax A and Heller E J 1997 *Phys. Rev.* E **56** 2496
[23] Vega J L, Uzer T and Ford J 1995 *Phys. Rev.* E **52** 1490